BNL-225761-2024-JAAM

GRP-COCA-34

Screening of Cu-Based Catalysts for Selective Methane to Methanol Conversion

E. Huang, P. Liu

To be published in "The Journal of Physical Chemistry C"

May 2024

Chemistry Department

Brookhaven National Laboratory

U.S. Department of Energy

USDOE Office of Science (SC), Basic Energy Sciences (BES)

Notice: This manuscript has been authored by employees of Brookhaven Science Associates, LLC under Contract No.DE-SC0012704 with the U.S. Department of Energy. The publisher by accepting the manuscript for publication acknowledges that the United States Government retains a non-exclusive, paid-up, irrevocable, world-wide license to publish or reproduce the published form of this manuscript, or allow others to do so, for United States Government purposes.

DISCLAIMER

This report was prepared as an account of work sponsored by an agency of the United States Government. Neither the United States Government nor any agency thereof, nor any of their employees, nor any of their contractors, subcontractors, or their employees, makes any warranty, express or implied, or assumes any legal liability or responsibility for the accuracy, completeness, or any third party's use or the results of such use of any information, apparatus, product, or process disclosed, or represents that its use would not infringe privately owned rights. Reference herein to any specific commercial product, process, or service by trade name, trademark, manufacturer, or otherwise, does not necessarily constitute or imply its endorsement, recommendation, or favoring by the United States Government or any agency thereof or its contractors or subcontractors. The views and opinions of authors expressed herein do not necessarily state or reflect those of the United States Government or any agency thereof.

Screening of Cu-based Catalysts for Selective Methane to Methanol Conversion

Erwei Huang[1], Ping Liu[1,2,*]

[1] Chemistry Division, Brookhaven National Laboratory, Upton, NY 11973, USA

[2] Department of Chemistry, Stony Brook University, Stony Brook, NY 11794, USA

[*] Corresponding author: pingliu3@bnl.gov (P. L.)

Abstract

Developing selective catalysts for methane conversion to added value chemicals has been considered as a promising approach for efficient utilization of abundant natural gas resources. Here, we present a descriptor-based screening for high methane conversion and methanol selectivity at the interfaces between metal oxide clusters and $Cu_2O/Cu(111)$ support ($MO_x/Cu_2O/Cu(111)$, M = Mg, Fe, Co, Ni, Cu, Zn, Ti, Zr, Sn, Ce) on exposure to the mixture of $CH_4/O_2/H_2O$. Wherein, the activation energy of direct methane to methanol conversion, $*OH + *CH_4 \rightarrow *CH_3OH + *H$, and the ratio for adsorption energy of oxygen and water, $E_{ads}(O_2)/E_{ads}(H_2O)$, are identified as the effective descriptor for methane conversion and methanol selectivity, respectively. By providing an exceptional oxygen and hydroxyl sites with high-lying O 2p states, the $MgO/Cu_2O/Cu(111)$ catalyst is found to be the most promising system among the systems studied, being able to provide the highest methane conversion with high methanol selectivity.

1. Introduction

The efficient utilization of abundant natural gas resources with main component as methane (CH_4) highly relies on the development of successful catalysts toward CH_4 reforming[1-4]. Wherein, the selective methane to methanol ($CH_4 \rightarrow CH_3OH$) has attracted extensive interests due to its advantage in achieving an energy-efficient one-step conversion with high CH_3OH selectivity compared with the conventional syngas pathway[3, 5]. Enzyme works efficiently under natural environment.[6, 7]. However, so far, no industrial catalyst is available. Instead, the bio-mimic zeolites with specific member-rings [8, 9] and complex metal oxides with unique interfaces[10-15] have been studied for potential applications in industry. Nevertheless, developing and screening viable catalysts to enable active and selective $CH_4 \rightarrow CH_3OH$ conversion under practical conditions in industry has long been challenging due to the limited understanding of such complex catalysis[5, 16].

Previously, Nørskov et. al. demonstrated that the catalyst screening using descriptors is very effective to discover advanced catalysts at a theoretical level[5, 16-21]. Following the same scheme, here we perform a descriptor-based screening using density functional theory (DFT), seeking for highly active and selective $MO_x/Cu_2O/Cu(111)$ (M = Ce, Zn, Sn to M=Mg, Fe, Co, Ni, Cu, Ti, Zr) model catalysts on exposure to a mixture of $CH_4/O_2/H_2O$. In our study, M of MO_x is chosen to cover a wide range of metals, which includes s-block element (Mg), p-block element (Sn), d-block elements (Fe, Co, Ni, Cu, Zn, Ti, Zr), and f-block element (Ce). This enables us to gain better understanding of the effect of intrinsic property of M on the catalysis over $MO_x/Cu_2O/Cu(111)$. The screening is built on our previous studies using DFT and kinetic modeling, showing that the CH_4 oxidation catalysis over the model $Cu_2O/Cu(111)$ substrate could be tuned by depositing secondary metal oxide clusters, MO_x, (M = Ce, Zn, Sn), to form the inverse catalysts $MO_x/Cu_2O/Cu(111)$ catalysts[11-15, 22]. Based on these previous results, we identify the

effective descriptor that scale well with the CH_4 conversion, i.e. barrier for the elementary step $*OH + *CH_4 \rightarrow *CH_3OH + *H$, using degree of rate control (DRC), a mathematical approach for analyzing multistep reaction mechanisms[23-27]. The ratio of O_2/H_2O adsorption energy, $E_{ads}(O_2)/E_{ads}(H_2O)$, is selected as the selectivity descriptor, which correlates the CH_3OH selectivity via a negative linear regression at the MO_x-Cu_2O (M = Ce, Zn, Sn) interfaces according to our previous studies[14, 15]. Based on the identified descriptors, the deposition of MgO cluster is identified to show the most significant enhancement in CH_4 conversion and CH_3OH selectivity of Cu_2O/Cu(111) among all the systems studied.

2. Computational Methods

A spin polarized density functional theory (DFT)[28, 29] implemented in Vienna *ab initio* simulation package (VASP)[30] was used to perform all the calculations. A 400eV kinetic energy cutoff and the projector augmented wave method (PAW)[31, 32] together with GGA exchange-correlation functional plus the PBE functional[33] were employed. Monkhorst-Pack[34] meshes with 3×3×1 were used to sample the Brillouin zone for all the surface calculations while gamma point were employed for all gas-phase species. The nudged elastic band method (NEB)[35] for each elementary reaction intermediates were performed to derive the transition states. The criteria for total energies and forces on all atoms were set as 10^{-5} eV and 0.02 eV $Å^{-1}$ for convergence, respectively. Gaussian smearing with width 0.05 eV was used to improve the convergence. The dispersion forces were not considered here due to the overestimation the strong interactions, e.g. water and oxygen, which represent a major part of the reaction network and thus the activity/selectivity, according to our previous studies[11-13].

$MO_x/Cu_2O/Cu(111)$ catalyst was simulated with a 3 layer of 4×4 Cu(111) surface and one monolayer of Cu_xO ($x \approx 1.13$) with M_3O_3 or M_3O_6 cluster deposited on top (Figure S1 and Figure S2). The Mg(2p, 3s), Fe(3p, 3d, 4s), Co(3p, 3d, 4s), Ni (3p, 3d, 4s), Cu (3p, 3d, 4s), Zn(3d, 4s), Ti(3p, 3d, 4s), Zr(4s, 4p, 4d,5s), Sn (4d, 5s, 5p), Ce(4f, 5d, 6s), C (2s, 2p), O (2s, 2p) and H (1s) electrons were treated as valence states, while the remaining electrons were kept frozen as core states. The Hubbard-like U term[36] was considered to address Cu 3d electrons for the Cu_xO surface ($U_{eff} = 5.2$)[11], Fe_3O_3 cluster ($U_{eff} = 5.3$)[37], Co_3O_3 cluster ($U_{eff} = 3.32$)[37], Ni_3O_3 cluster ($U_{eff} = 6.2$)[37], Cu_3O_3 cluster ($U_{eff} = 5.2$)[11], Ti_3O_6 cluster ($U_{eff} = 4.5$)[38], Ce_3O_6 cluster ($U_{eff} = 4.5$)[11], in which the Coulomb U and exchange J parameters were combined into a single parameter $U_{eff} = U - J$. During DFT optimizations, the bottom two layers were fixed while the rest were allowed to relax with adsorbates. We calculated the binding energies (E_b) of MO_x clusters on $Cu_2O/Cu(111)$, and the results showed that the deposition of MO_x was thermodynamically preferred. Among $MO_x/Cu_2O/Cu(111)$ systems studied, Mg_3O_3 showed the strongest binding (E_b = -4.60 eV), which was gradually weakened on going to Zr_3O_6 (E_b = -3.91 eV), Ti_3O_6 (E_b = -3.80 eV), Sn_3O_6 (E_b = -3.75 eV), Fe_3O_3 (E_b = -3.63 eV), Ce_3O_6 (E_b = -2.98 eV), Ni_3O_3 (E_b = -2.69 eV) or Cu_3O_6 (E_b = -2.68 eV), Zn_3O_3 (E_b = -2.26 eV) and Co_3O_3 (E_b = -1.58 eV). Wherein, our previous studies in both theory and experiment indicated that the $Cu_2O/Cu(111)$-supported Ce_3O_6, Sn_3O_6 and Zn_3O_3 remained intact on exposure to CH_4, O_2 and H_2O at 450 K[12-15]. Different spin states were tested to optimize the supported MO_x on $Cu_2O/Cu(111)$, where the most stable configuration was used to study CH_4 activation (Figure S2).

Overall, the adsorption energy of adsorbate on the $MO_x/Cu_2O/Cu(111)$ model surface was calculated as:

$$E_{ads} = E(\text{Adsorbate/Surface}) - E(\text{Surface}) - E(\text{Adsorbate})$$

where E is the total energy obtained from DFT calculations incorporated with zero-point energy (ZPE) correction E_{ZPE}:

$$E_{ZPE} = \sum_{i}^{number\ of\ modes} \frac{1}{2} h\nu_i$$

where ν_i is DFT calculated vibrational frequency by harmonic normal mode approximation for each intermediate.

Campbell's degree of rate control (DRC_i, or X_i) was utilized to identify the key steps within a kinetic model for controlling the interested reaction rates via[23, 25-27]:

$$DRC_i = \mathrm{X}_i = \left(\frac{-\partial \ln r}{\partial \left(\frac{E_i}{RT} \right)} \right)_{E_{j \neq i}}$$

where r is the net reaction rate, and the partial derivative is taken holding constant the standard-state energy (E) of all other species, j. In addition, the conversion of X_i was considered over all elementary steps i involved in the kinetic model[24, 25, 27]:

$$\sum_{steps} \mathrm{X}_i = 1$$

A higher X_i represents a higher weight of the corresponding elementary step in controlling the reaction rates of interest.

The p-band center, which has been proposed and applied as a descriptor to predict catalytic activity[39], was calculated via:

$$\varepsilon_p^f = \frac{\int_{-\infty}^{0} n_p(\varepsilon)\varepsilon\, d\varepsilon}{\int_{-\infty}^{0} n_p(\varepsilon)\, d\varepsilon}$$

3. Results and Discussion

3.1 Screening for catalytic activity

Catalysts screening at a theoretical level strongly depends on the identification of effective descriptors that control catalytic performances toward the targeted reactions[2, 3, 5, 16, 26, 39-45]. Multiple descriptors have been developed to address the direct $CH_4 \rightarrow CH_3OH$ conversion either in heterogeneous catalysis or homogeneous catalysis[3, 5, 16, 46]. For example, Nørskov et. al. proposed that hydrogen affinity could be used to screen the activity toward C-H bond activation of CH_4 by the surface oxygen over large-range of catalysts[16], while the selectivity limit for $CH_4 \rightarrow CH_3OH$ process could be overcame by adopting strategies of CH_3OH collector, aqueous conditions, and diffusion limited systems[5].

Table 1. Reaction energy (ΔE) and activation energy (E_a) for $*OH + *CH_4 \rightarrow *CH_3OH + *H$ as well as the corresponding degree of rate control (DRC, X_i) for $Ce_3O_6/Cu_2O/Cu(111)$[12], $Zn_3O_3/Cu_2O/Cu(111)$[13] and $Sn_3O_6/Cu_2O/Cu(111)$[14] model surfaces.

	ΔE (eV)	E_a (eV)	X_i
$Ce_3O_6/Cu_2O/Cu(111)$	-0.81	0.97	0.66
$Zn_3O_3/Cu_2O/Cu(111)$	-0.44	1.12	0.80
$Sn_3O_6/Cu_2O/Cu(111)$	-0.81	1.00	0.69

Following the framework developed in our previous study[47], the descriptor is extracted based on the activation barriers (E_a) involved in the kinetic model in this study. Due to the limited

data points available, the DRC, rather than the machine learning method[47], is used to extract the effective descriptors based on the previously reported kinetic modeling of $CeO_2/Cu_2O/Cu(111)$[12], $ZnO/Cu_2O/Cu(111)$[13] and $SnO_2/Cu_2O/Cu(111)$[14] on exposure to the mixture of CH_4, O_2 and H_2O with a pressure ratio of 2:1:8 at 450 K. Here, for simplicity the similar MO_x-Cu_2O interfacial structures, i.e. a trimer, M_3O_{3y}, deposited on a $Cu_2O/Cu(111)$ surface, are considered, which was found to follow the same reaction pathway for CH_4 oxidation by O_2 and H_2O previously.

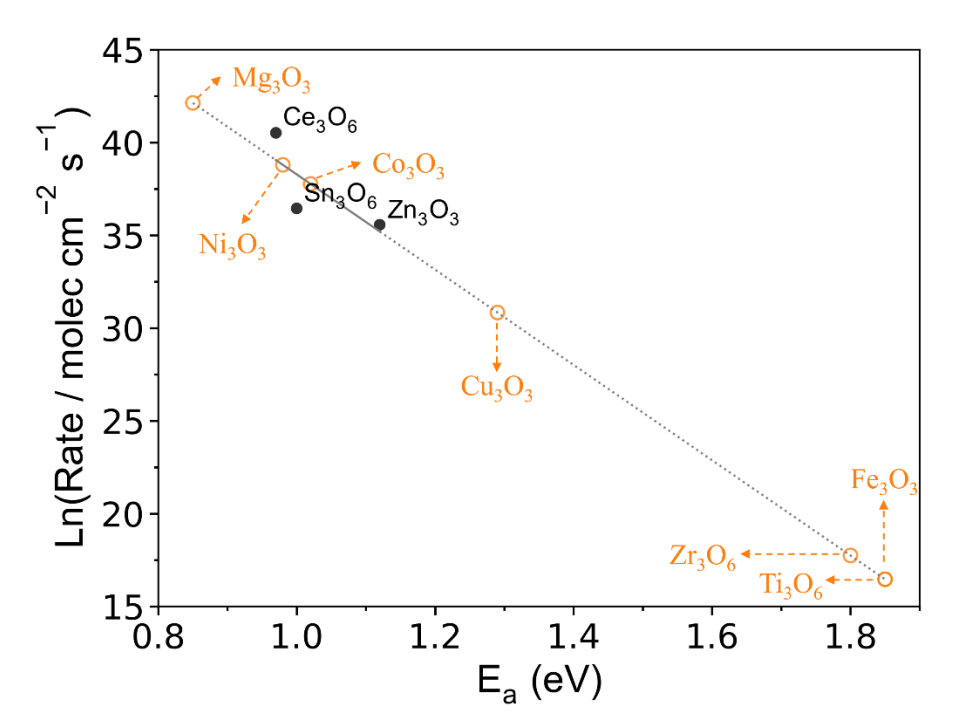

Figure 1. Correlation between the natural logarithm of simulated methane conversion rate on exposure to a gas mixture of CH_4, O_2 and H_2O with a pressure ratio of 2:1:4 at 450K and the activation energy (E_a) of $*OH + *CH_4 \rightarrow *CH_3OH + *H$. The black filled spheres represent the data points for $Ce_3O_6/Cu_2O/Cu(111)$[12], $Zn_3O_3/Cu_2O/Cu(111)$[13] and $Sn_3O_6/Cu_2O/Cu(111)$[14] calculated in our previous work, and the black line stands for the corresponding linear regression; The orange hollow sphere represents the data points for other $MO_x/Cu_2O/Cu(111)$ systems, where

the methane conversion rate is predicted based on DFT-calculated E_a using the extrapolated linear regression (black line).

For all three systems, the value of DRC for E_a of *OH + *CH_4 → *CH_3OH + *H is the dominant among the elementary steps involved (X_i > 0.65, Table 1). That is, the CH_4 oxidation rate by O_2 and H_2O likely depends on the C-H bond scission of *CH_4 by the surface *OH to form *CH_3OH. Indeed, Figure 1 shows a negative linear regression (sloid back line) between E_a of *OH + *CH_4 → *CH_3OH + *H and the natural logarithm of KMC-simulated CH_4 conversion rates on $Ce_3O_6/Cu_2O/Cu(111)$, $Zn_3O_3/Cu_2O/Cu(111)$ and $Sn_3O_6/Cu_2O/Cu(111)$[11-15]. In general, a lower value of E_a corresponds to a higher CH_4 conversion rate on $MO_x/Cu_2O/Cu(111)$. Among the three systems, $Ce_3O_6/Cu_2O/Cu(111)$ shows the lowest value (E_a = 0.97 eV) and the highest CH_4 conversion rate; while $Sn_3O_6/Cu_2O/Cu(111)$ (E_a = 1.00 eV) and $Zn_3O_3/Cu_2O/Cu(111)$ (E_a = 1.12 eV) were less active with higher activation barrier (Figure 1).

Using the identified descriptor, E_a for *OH + *CH_4 → *CH_3OH + *H, we screen the CH_4 conversion over the $MO_x/Cu_2O/Cu(111)$ (M = Mg, Fe, Co, Ni, Cu, Ti, Zr) systems, which has not been studied. The candidate MO_x clusters considered for deposition on $Cu_2O/Cu(111)$ were reported previously as promising candidates for CH_4 activation/conversion. Specifically, FeO_x and CuO_x clusters were chosen due to their encouraging performance for CH_4 to CH_3OH conversion in either enzymes[6, 7, 48-50] or zeolites[8, 9, 51-59]. CoO_x and NiO_x clusters were also predicted as possible active centers for CH_4 conversion in zeolites[60, 61]. Finally, TiO_2[62] and ZrO_2[63, 64], and MgO[65, 66] were reported as a good support for the C-H bond scission of CH_4. Again, the same interface structures as $MO_x/Cu_2O/Cu(111)$ (M=Ce, Zn, Sn) is adopted by depositing Mg_3O_3, Fe_3O_3, Co_3O_3, Ni_3O_3, Cu_3O_3, Ti_3O_6 and Zr_3O_6 clusters on $Cu_2O/Cu(111)$ substrate (Figure 2).

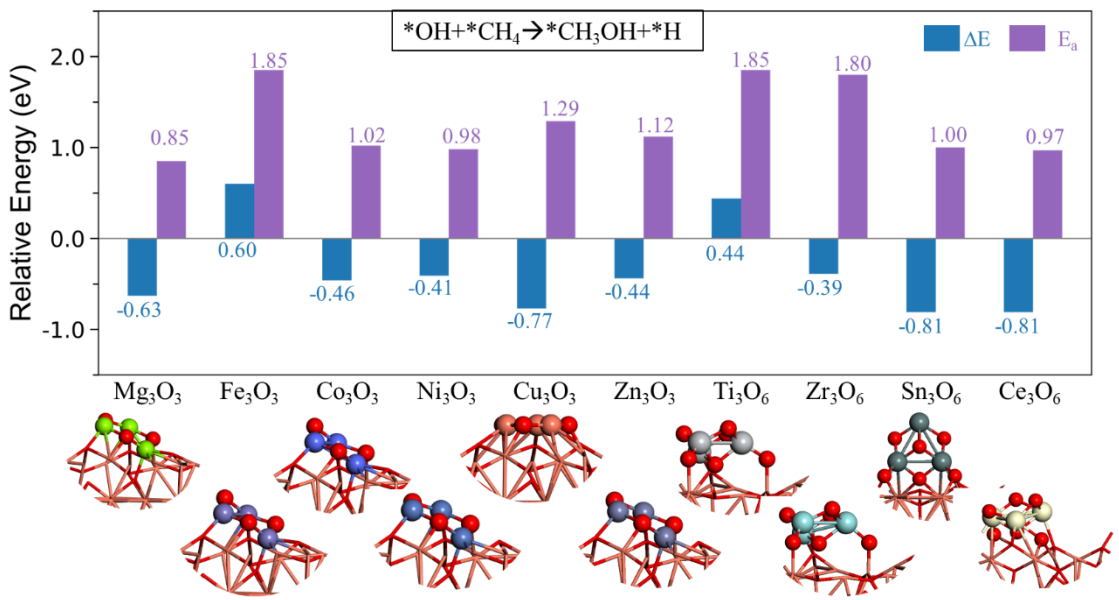

Figure 2. DFT-calculated reaction energy (ΔE) and activation energy (E_a) of *OH + *CH_4 → *CH_3OH + *H for all $MO_x/Cu_2O/Cu(111)$ systems ($Mg_3O_3/Cu_2O/Cu(111)$, $Fe_3O_3/Cu_2O/Cu(111)$, $Co_3O_3/Cu_2O/Cu(111)$, $Ni_3O_3/Cu_2O/Cu(111)$, $Cu_3O_3/Cu_2O/Cu(111)$, $Zn_3O_3/Cu_2O/Cu(111)$, $Ti_3O_6/Cu_2O/Cu(111)$, $Zr_3O_6/Cu_2O/Cu(111)$, $Sn_3O_6/Cu_2O/Cu(111)$ and $Ce_3O_6/Cu_2O/Cu(111)$). The corresponding DFT-optimized structures are shown in the lower panel and Figures S1-2. See Figure S3 for top and side view of optimized structures for initial state (IS), transition state (TS) and final state (FS) involved in each reaction. Red: O; Green: Mg; Dark purple: Fe; Dark blue: Co; Light purple: Ni; Brown: Cu; Violet: Zn; Bright grey: Ti; Cyan: Zr; Dark green: Sn; Yellow: Ce.

According to the DFT calculations, $Mg_3O_3/Cu_2O/Cu(111)$ demonstrates the lowest barrier for *OH + *CH_4 → *CH_3OH + *H (E_a = 0.85 eV), which is followed by $Ni_3O_3/Cu_2O/Cu(111)$ (E_a = 0.98 eV) < $Co_3O_3/Cu_2O/Cu(111)$ (E_a = 1.02 eV) < $Cu_3O_3/Cu_2O/Cu(111)$ (E_a = 1.29 eV) < $Zr_3O_6/Cu_2O/Cu(111)$ (E_a = 1.80 eV) < $Ti_3O_6/Cu_2O/Cu(111)$ (E_a = 1.85 eV) < $Fe_3O_3/Cu_2O/Cu(111)$ (E_a = 1.85 eV) in an increasing sequence. Based on the extrapolated linear regression (black line, Figure 1), the CH_4 conversion rates are roughly estimated using the calculated E_a for a new

$MO_x/Cu_2O/Cu(111)$ system (open orange circle). $Mg_3O_3/Cu_2O/Cu(111)$ is found to be the only system showing a higher CH_4 conversion rate than the most active $Ce_3O_6/Cu_2O/Cu(111)$ model previously reported (Figure 1)[12]. $Ni_3O_3/Cu_2O/Cu(111)$ can also be considered as an alternative candidate, which displays a conversion rate slightly less than $Ce_3O_6/Cu_2O/Cu(111)$. While the systems, e.g. $Fe_3O_3/Cu_2O/Cu(111)$, $Zr_3O_6/Cu_2O/Cu(111)$, and $Ti_3O_6/Cu_2O/Cu(111)$, are predicted to be much less active in terms of CH_4 conversion. An intermediate activity is expected for $Cu_3O_3/Cu_2O/Cu(111)$. While a different structure was reported previously for Cu_3O_3 on interaction with rutile (110) surfaces of TiO_2, SnO_2 and RuO_2, which provided an active oxygen site to directly oxidize CH_4 to CH_3OH[67]. Note that, in the case that the other elementary steps along the pathway control the conversion more significantly than $*OH + *CH_4 \rightarrow *CH_3OH + *H$, the activity is likely further decreased for $MO_x/Cu_2O/Cu(111)$ (M = Fe, Co, Ni, Cu, Ti, Zr) systems, which have been screened to be less active than $Ce_3O_6/Cu_2O/Cu(111)$ (Figure 1). While the dominancy of $*OH + *CH_4 \rightarrow *CH_3OH + *H$ and thus the screened superior activity for $CH_4 \rightarrow CH_3OH$ conversion is necessary to be validated for $Mg_3O_3/Cu_2O/Cu(111)$, as demonstrated below.

3.2 Screening for catalytic selectivity

Different from the catalytic activity shown above, the DRC analysis for selectivity does not identify the barrier of any elementary step involved in the kinetic model that corresponds to a relatively high DRC value ($X_i > 0.5$). That is, none of the elementary steps is capable of controlling the CH_3OH selectivity individually, while the descriptors that involve the contributions from two or more elementary steps may be more effective. Indeed, a negative linear regression between the CH_3OH selectivity and $E_{ads}(O_2)/E_{ads}(H_2O)$ was found at the MO_x-Cu_2O (M=Ce, Zn, Sn) interface according to our previous study.[14] Specifically, the system, which selectively binds O_2 weakly and

H_2O strongly, as seen for $SnO_2/Cu_2O/Cu(111)$, helps prevent O_2 adsorption and dissociation at the active sites, thus resulting in the high CH_3OH selectivity (Figure 3).

Following the same scheme as the case for screening the CH_4 conversion rate, $E_{ads}(O_2)/E_{ads}(H_2O)$ is calculated for the $MO_x/Cu_2O/Cu(111)$ systems using DFT (Figures S4-S6), and the corresponding CH_3OH selectivity is estimated based on the extrapolated linear regression (black line, Figure 4). According to the DFT results, all the screened systems show a higher value of $E_{ads}(O_2)/E_{ads}(H_2O)$ than the most selective $Sn_3O_6/Cu_2O/Cu(111)$ model previously reported[14]. Thus, lower CH_3OH selectivity is expected. Yet, the corresponding values for $Ni_3O_3/Cu_2O/Cu(111)$ (0.35), $Cu_3O_3/Cu_2O/Cu(111)$ (0.36), $Mg_3O_3/Cu_2O/Cu(111)$ (0.44) and $Co_3O_3/Cu_2O/Cu(111)$ (0.46) are still low, and the corresponding CH_3OH selectivity is likely to remain high (> 98%, Figure 3), which is higher than that on $Ce_3O_6/Cu_2O/Cu(111)$.

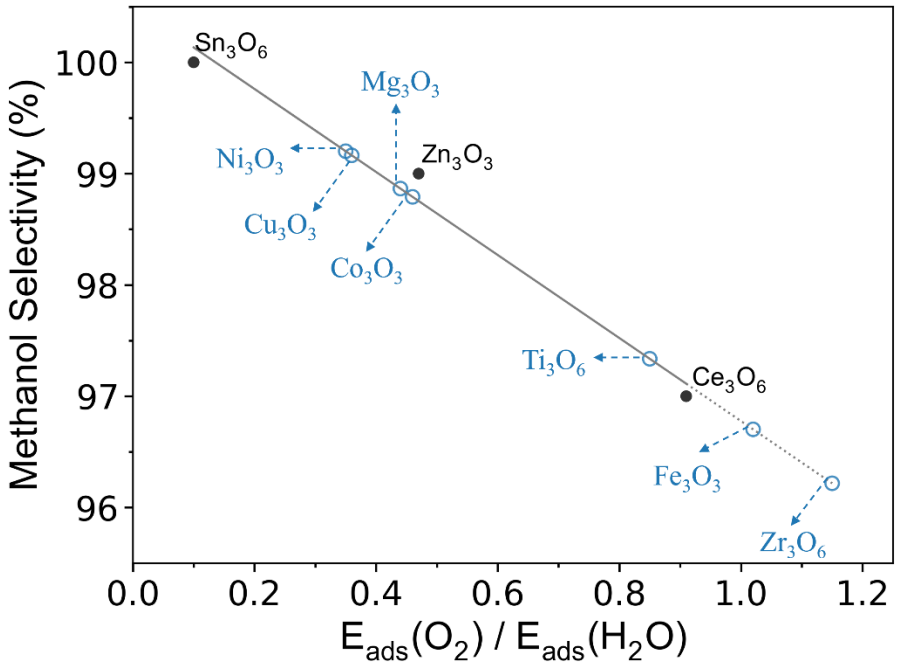

Figure 3. Correlation between methanol selectivity on exposure to a gas mixture of CH_4, O_2 and H_2O with a pressure ratio of 2:1:4 at 450K and the ratio of O_2/H_2O adsorption energy, $E_{ads}(O_2)/E_{ads}(H_2O)$, at the MO_x-Cu_2O interface. The black filled spheres represent the data points for $Ce_3O_6/Cu_2O/Cu(111)$, $Zn_3O_3/Cu_2O/Cu(111)$ and $Sn_3O_6/Cu_2O/Cu(111)$ calculated in our previous work; The black line stands for the linear regression based on the results of $Ce_3O_6/Cu_2O/Cu(111)$, $Zn_3O_3/Cu_2O/Cu(111)$ and $Sn_3O_6/Cu_2O/Cu(111)$. The blue hollow sphere represents the data points for other $MO_x/Cu_2O/Cu(111)$ systems, where the methanol selectivity is predicted based on DFT-calculated $E_{ads}(O_2)/E_{ads}(H_2O)$ using the extrapolated linear regression (black line).

3.3 Confirmation for screened optimal catalyst

According to the descriptor-based screening of activity and selectivity for CH_4 oxidation by O_2 and H_2O, $Mg_3O_3/Cu_2O/Cu(111)$ is the only system that likely display higher activities than the previously reported $MO_x/Cu_2O/Cu(111)$ systems [12-15], while still maintaining the high CH_3OH selectivity. To confirm the screening results, DFT calculations are further performed to determine the potential diagram for conversion of CH_4 to CH_3OH by H_2O on $Mg_3O_3/Cu_2O/Cu(111)$ (Figure 4). Note that, O_2 is not included here, which was found previously to only help recover the oxygen vacancies generated by removal of *OH and thus stabilize active MO_x during the reaction at the MO_x-Cu_2O (M=Ce, Zn, Sn) interfaces[12-15, 68].

The Mg_3O_3-Cu_2O interface initiates the reaction via a highly exothermic (ΔE = -1.56 eV) and spontaneous H_2O dissociation, which limits the O_2 dissociation at these active sites to produce CO_2 via a complete oxidation. The generated *OH species at the Mg site are active enough to enable the facile C-H bond scission of $*CH_4$ and directly produce $*CH_3OH$ (E_a = 0.85 eV, ΔE = -

0.63 eV). While *CH_3OH prefers the dehydrogenation to *CH_3O (ΔE = -0.98 eV), rather than desorption (ΔE = 0.95 eV). However, further decomposition is hindered by the presence of H_2O. A facile extraction process is achieved via a CH_3O···HOH motif (E_a = 0.24 eV, ΔE = 0.19 eV), resulting in the facilitated formation of *CH_3OH and sequential *CH_3OH desorption from the interfacial MgO-Cu_2O sites (E_a = 0.54 eV). Thus, the DFT calculations confirm the prediction from descriptor-based screening. That is, the Mg_3O_3/Cu_2O/Cu(111) model catalyst is a promising catalyst on exposure to CH_4/O_2/H_2O, not only enabling the CH_4 conversion in a rate higher, but also providing a higher CH_3OH selectivity than previously reported Ce_3O_6/Cu_2O/Cu(111). As seen previously on CeO_2-Cu_2O, ZnO-Cu_2O, and SnO_2-Cu_2O interfacial sites[12-15], H_2O plays an essential role during this process, blocking active site from competing O_2 dissociation, providing active *OH species and extracting *CH_3OH from the surface, to ensure the overall selective $CH_4 \rightarrow CH_3OH$ pathway at the MgO-Cu_2O interfaces (Figure 4).

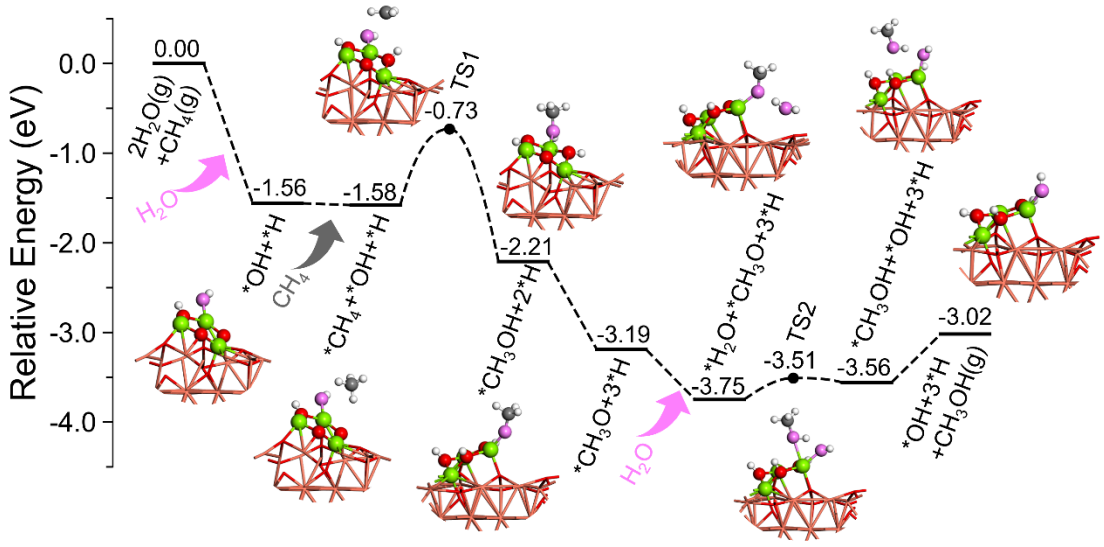

Figure 4. Potential energy diagram for selective CH_4 oxidation to CH_3OH on Mg_3O_3/Cu_2O/Cu(111) model catalyst. Inset: DFT-optimized structures for intermediates and transition state (TS)

involved. See Figure S7 for corresponding top and side views. Brown: Cu; Green: Mg; Red: O; Purple: O (from H_2O); Grey: C; White: H.

Among the systems studied, the highest CH_4 conversion rate predicted for $Mg_3O_3/Cu_2O/Cu(111)$ is likely associated its exceptionally high-lying O 2p for both oxygen in the supported Mg_3O_3 cluster and the dissociated *OH fragment at the Mg site from H_2O (Figure 5). Due to a lower electronegativity Mg than other M of $MO_x/Cu_2O/Cu(111)$, the Mg site of deposited Mg_3O_3 displays a strong affinity to oxygen-anchored species. This is well demonstrated by the spontaneous H_2O dissociation (Figure 4), and the produced *OH fragment binds Mg strongly, resulting in significant variation of Mg 2p states and formation of Mg hydroxide-like species that is featured with high-lying O 2p states (Figure S8). The synergy between the oxygen and resulted hydroxyl sites over Mg_3O_3 is observed to stabilize the dissociated *H in the form of *OH and $*CH_3$ in the form of $*CH_3OH$, facilitating the rate limiting CH_4 activation via $*OH + *CH_4 \rightarrow *CH_3OH + *H$ (Figure 4). By comparison, the effect of forming M-OH bond is much less, and the O 2p positions for other MO_x clusters are further away from the Fermi level, thus the higher reaction energies and barriers for $*OH + *CH_4 \rightarrow *CH_3OH + *H$, are observed and lower methane conversions are expected (Figures 1, 2 and 5). Here, the presence of H_2O opens a pathway, where the direct $CH_4 \rightarrow CH_3OH$ conversion only depends on the oxygen and hydroxyl sites of $MO_x/Cu_2O/Cu(111)$. Thus, the higher the corresponding O 2p states, the higher the activity. While without H_2O, a moderate O 2p state was found to be necessary for optimizing the selective CH_3OH production from CH_4 dissociation at the Cu-O hybrid sites of CuO_x-based systems[67, 69]. Note that $Ce_3O_6/Cu_2O/Cu(111)$, $Sn_3O_6/Cu_2O/Cu(111)$ and $Cu_3O_3/Cu_2O/Cu(111)$ are exceptions. Despite of the lower lying O 2p states (Figure 5), the reaction, $OH + *CH_4 \rightarrow *CH_3OH + *H$, is more thermodynamically favorable (ΔE = -0.81 eV for M = Ce, -0.81 eV for M = Sn, -0.71 eV for M =

Cu) than that of $Mg_3O_3/Cu_2O/Cu(111)$. Yet the activation barrier (E_a = 0.97 eV for M = Ce, 1.00 eV for M = Sn, 1.29 eV for M = Cu) is still higher. Wherein, the significant structural fluxionality of MO_x clusters on interaction with the adsorbates contributes to enhanced stabilization to the final states, while the impact on the saddle transition states is less.

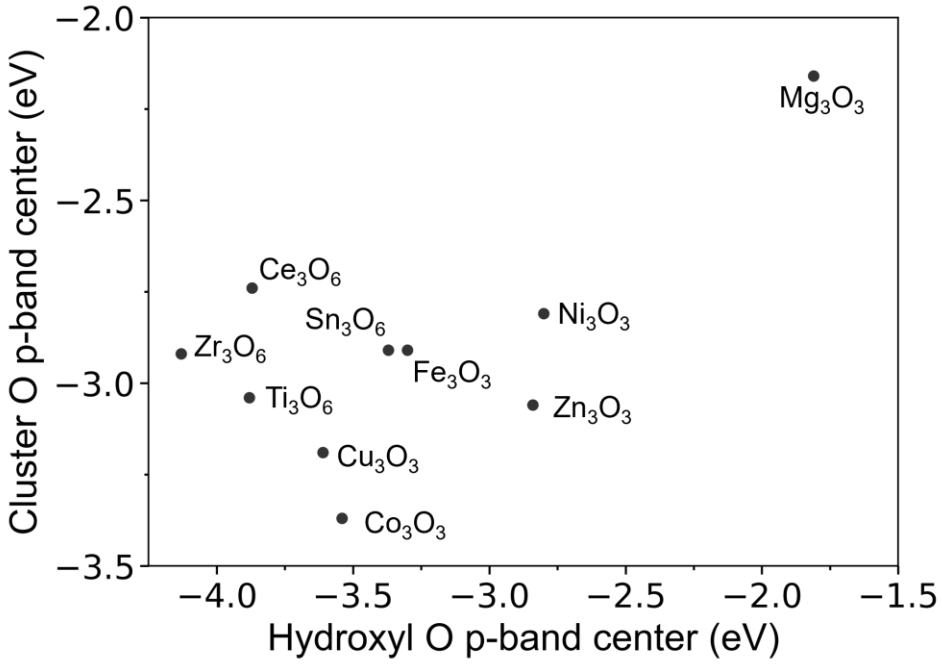

Figure 5. Calculated center of O 2p states for the hydroxyl and oxygen species on $MO_x/Cu_2O/Cu(111)$ systems. The hydroxyl species is from H_2O dissociation at the M site and oxygen species is from MO_x cluster. Both sites participate in the CH_4 dissociation at the MO_x-Cu_2O interface.

4. Conclusions

We perform the descriptor-based screening of $MO_x/Cu_2O/Cu(111)$ (M = Mg, Fe, Co, Ni, Cu, Ti, Zr) model systems based on the DFT calculations, seeking to advance catalysts towards high CH_4 conversion and high CH_3OH selectivity on exposure the mixture of CH_4, O_2 and H_2O.

Using the degree of rate control analysis, the activation energy of *OH + *CH_4 → *CH_3OH + *H is identified as the effective descriptor for the CH_4 conversion. In addition, the binding energy ratio of O_2/H_2O, $E_{ads}(O_2)/E_{ads}(H_2O)$, at the MO_x-Cu_2O interface is utilized to estimate the CH_3OH selectivity.

$MgO/Cu_2O/Cu(111)$ is screened as the only catalyst among the systems studied, which is predicted to show a higher CH_4 conversion rate and CH_3OH selectivity than the active $Ce_3O_6/Cu_2O/Cu(111)$ reported previously. The DFT calculation of potential energy diagram confirms this prediction, showing a facile H_2O dissociation to form active *OH, CH_4 oxidation by *OH to form *CH_3OH and removal of *CH_3O to produce CH_3OH at the MgO-Cu_2O interface. The superior catalytic behavior of $MgO/Cu_2O/Cu(111)$ depends on the exceptionally high activity of oxygen and hydroxyl species provided at the interface, being able to facilitate H_2O dissociation and selective oxidation of CH_4 to CH_3OH.

Supporting Information

Supplementary figures, including DFT-optimized structures of reaction intermediates and transition states involved in selective methane oxidation to methanol; DFT-calculated binding energies.

Acknowledgments

This research was conducted at the Chemistry Division at Brookhaven National Laboratory (BNL) and was supported by the Division of Chemical Science, Geoscience, and Bioscience, Office of Basic Energy Science of the US Department of Energy (DOE) under Contract No. DE-SC0012704 through BNL-FWP CO-040. The DFT calculations were performed using computational resources at the Center for Functional Nanomaterials (CFN), a component of the

Computational Science Initiative, at BNL under contract no. DE-SC0012704, and at the National Energy Research Scientific Computing Center (NERSC), a U.S. DOE Office of Science User Facility located at Lawrence Berkeley National Laboratory, operated under Contract No. DE-AC02-05CH11231.

Notes

The authors declare no competing financial interest.

References

1. Wang, Q.; Chen, X.; Jha, A. N.; Rogers, H., Natural gas from shale formation – The evolution, evidences and challenges of shale gas revolution in United States. *Renewable Sustainable Energy Rev.* **2014,** *30*, 1-28.
2. Chen, S.; Zaffran, J.; Yang, B., Descriptor design in the computational screening of Ni-based catalysts with balanced activity and stability for dry reforming of methane reaction. *ACS Catal.* **2020,** *10* (5), 3074-3083.
3. Nandy, A.; Duan, C.; Goffinet, C.; Kulik, H. J., New strategies for direct methane-to-methanol conversion from active learning exploration of 16 million catalysts. *JACS Au* **2022,** *2* (5), 1200-1213.
4. Huang, E.; Rui, N.; Rosales, R.; Liu, P.; Rodriguez, J. A., Activation and conversion of methane to syngas over ZrO2/Cu(111) catalysts near room temperature. *J. Am. Chem. Soc.* **2023,** *145* (15), 8326-8331.
5. Latimer, A. A.; Kakekhani, A.; Kulkarni, A. R.; Nørskov, J. K., Direct methane to methanol: The selectivity–conversion limit and design strategies. *ACS Catal.* **2018**, 6894-6907.
6. Sirajuddin, S.; Rosenzweig, A. C., Enzymatic oxidation of methane. *Biochemistry* **2015,** *54* (14), 2283-2294.
7. Wang, V. C. C.; Maji, S.; Chen, P. P. Y.; Lee, H. K.; Yu, S. S. F.; Chan, S. I., Alkane oxidation: Methane monooxygenases, related enzymes, and their biomimetics. *Chem. Rev.* **2017,** *117* (13), 8574-8621.
8. Snyder, B. E. R.; Bols, M. L.; Schoonheydt, R. A.; Sels, B. F.; Solomon, E. I., Iron and copper active sites in zeolites and their correlation to metalloenzymes. *Chem. Rev.* **2018,** *118* (5), 2718-2768.
9. Newton, M. A.; Knorpp, A. J.; Sushkevich, V. L.; Palagin, D.; van Bokhoven, J. A., Active sites and mechanisms in the direct conversion of methane to methanol using Cu in zeolitic hosts: a critical examination. *Chem. Soc. Rev.* **2020,** *49* (5), 1449-1486.
10. Lustemberg, P. G.; Palomino, R. M.; Gutierrez, R. A.; Grinter, D. C.; Vorokhta, M.; Liu, Z.; Ramirez, P. J.; Matolin, V.; Ganduglia-Pirovano, M. V.; Senanayake, S. D.; Rodriguez, J. A., Direct conversion of methane to methanol on Ni-Ceria surfaces: Metal-support interactions and water-enabled catalytic conversion by site blocking. *J. Am. Chem. Soc.* **2018,** *140* (24), 7681-7687.

11. Zuo, Z.; Ramírez, P. J.; Senanayake, S. D.; Liu, P.; Rodriguez, J. A., Low-temperature conversion of methane to methanol on CeOx/Cu2O catalysts: Water controlled activation of the C–H bond. *J. Am. Chem. Soc.* **2016,** *138* (42), 13810-13813.
12. Liu, Z.; Huang, E.; Orozco, I.; Liao, W.; Palomino, R. M.; Rui, N.; Duchoň, T.; Nemšák, S.; Grinter, D. C.; Mahapatra, M.; Liu, P.; Rodriguez, J. A.; Senanayake, S. D., Water-promoted interfacial pathways in methane oxidation to methanol on a CeO2-Cu2O catalyst. *Science* **2020,** *368* (6490), 513-517.
13. Huang, E.; Orozco, I.; Ramirez, P. J.; Liu, Z.; Zhang, F.; Mahapatra, M.; Nemsak, S.; Senanayake, S. D.; Rodriguez, J. A.; Liu, P., Selective methane oxidation to methanol on ZnO/Cu2O/Cu(111) catalysts: Multiple site-dependent behaviors. *J. Am. Chem. Soc.* **2021,** *143* (45), 19018-19032.
14. Huang, E.; Rui, N.; Rosales, R.; Kang, J.; Nemšák, S.; Senanayake, S. D.; Rodriguez, J. A.; Liu, P., Highly selective methane to methanol conversion on inverse SnO2/Cu2O/Cu(111) catalysts: Unique properties of SnO2 nanostructures and the inhibition of the direct oxidative combustion of methane. *ACS Catal.* **2022,** *12* (18), 11253-11262.
15. Huang, E.; Liu, P., Theoretical perspective of promoting direct methane-to-methanol conversion at complex metal oxide–metal interfaces. *J. Phys. Chem. Lett.* **2023,** *14* (29), 6556-6563.
16. Latimer, A. A.; Kulkarni, A. R.; Aljama, H.; Montoya, J. H.; Yoo, J. S.; Tsai, C.; Abild-Pedersen, F.; Studt, F.; Norskov, J. K., Understanding trends in C-H bond activation in heterogeneous catalysis. *Nat Mater* **2017,** *16* (2), 225-229.
17. Nørskov, J. K.; Abild-Pedersen, F.; Studt, F.; Bligaard, T., Density functional theory in surface chemistry and catalysis. *Proc. Natl. Acad. Sci.* **2011,** *108* (3), 937-943.
18. Latimer, A. A.; Aljama, H.; Kakekhani, A.; Yoo, J. S.; Kulkarni, A.; Tsai, C.; Garcia-Melchor, M.; Abild-Pedersen, F.; Norskov, J. K., Mechanistic insights into heterogeneous methane activation. *Phys. Chem. Chem. Phys.* **2017,** *19* (5), 3575-3581.
19. Aljama, H.; Nørskov, J. K.; Abild-Pedersen, F., Theoretical Insights into Methane C–H Bond Activation on Alkaline Metal Oxides. *J. Phys. Chem. C* **2017,** *121* (30), 16440-16446.
20. Nørskov, J. K.; Bligaard, T.; Rossmeisl, J.; Christensen, C. H., Towards the computational design of solid catalysts. *Nat. Chem.* **2009,** *1*, 37.
21. Medford, A. J.; Vojvodic, A.; Hummelshøj, J. S.; Voss, J.; Abild-Pedersen, F.; Studt, F.; Bligaard, T.; Nilsson, A.; Nørskov, J. K., From the Sabatier principle to a predictive theory of transition-metal heterogeneous catalysis. *J. Catal.* **2015,** *328*, 36-42.
22. Kang, J.; Rui, N.; Huang, E.; Tian, Y.; Mahapatra, M.; Rosales, R.; Orozco, I.; Shi, R.; Senanayake, S. D.; Liu, P.; Rodriguez, J. A., Surface characterization and methane activation on SnOx/Cu2O/Cu(111) inverse oxide/metal catalysts. *Phys. Chem. Chem. Phys.* **2021,** *23* (32), 17186-17196.
23. Campbell, C. T., Future directions and industrial perspectives micro- and macro-kinetics: Their relationship in heterogeneous catalysis. *Top. Catal.* **1994,** *1* (3), 353-366.
24. Barański, A., On the usefulness of Campbell's concept of the rate-determining step. *Solid State Ionics* **1999,** *117* (1), 123-128.
25. Stegelmann, C.; Andreasen, A.; Campbell, C. T., Degree of rate control: How much the energies of intermediates and transition states control rates. *J. Am. Chem. Soc.* **2009,** *131* (23), 8077-8082.
26. Wolcott, C. A.; Medford, A. J.; Studt, F.; Campbell, C. T., Degree of rate control approach to computational catalyst screening. *J. Catal.* **2015,** *330*, 197-207.

27. Campbell, C. T., The degree of rate control: A powerful tool for catalysis research. *ACS Catal.* **2017,** *7* (4), 2770-2779.
28. Hohenberg, P.; Kohn, W., Inhomogeneous electron gas. *Phys. Rev.* **1964,** *136* (3B), B864-B871.
29. Kohn, W.; Sham, L. J., Self-consistent equations including exchange and correlation effects. *Phys. Rev.* **1965,** *140* (4A), A1133-A1138.
30. Kresse, G.; Furthmuller, J., Efficient iterative schemes for ab initio total-energy calculations using a plane-wave basis set. *Phys. Rev. B* **1996,** *54* (16), 11169-11186.
31. Blochl, P. E., Projector augmented-wave method. *Physi. Rev. B* **1994,** *50* (24), 17953-17979.
32. Kresse, G.; Joubert, D., From ultrasoft pseudopotentials to the projector augmented-wave method. *Phys. Rev. B* **1999,** *59* (3), 1758-1775.
33. Perdew, J. P.; Burke, K.; Ernzerhof, M., Generalized gradient approximation made simple. *Phys. Rev. Lett.* **1996,** *77* (18), 3865-3868.
34. Monkhorst, H. J.; Pack, J. D., Special points for Brillouin-zone integrations. *Phys. Rev. B* **1976,** *13* (12), 5188-5192.
35. Henkelman, G.; Jonsson, H., Improved tangent estimate in the nudged elastic band method for finding minimum energy paths and saddle points. *J. Chem. Phys.* **2000,** *113* (22), 9978-9985.
36. Dudarev, S. L.; Botton, G. A.; Savrasov, S. Y.; Humphreys, C. J.; Sutton, A. P., Electron-energy-loss spectra and the structural stability of nickel oxide: An LSDA+U study. *Phys. Rev. B* **1998,** *57* (3), 1505-1509.
37. MaterialsProject. *https://materialsproject.org/ Accessed Online 2022-10-08*.
38. Baber, A. E.; Yang, X.; Kim, H. Y.; Mudiyanselage, K.; Soldemo, M.; Weissenrieder, J.; Senanayake, S. D.; Al-Mahboob, A.; Sadowski, J. T.; Evans, J.; Rodriguez, J. A.; Liu, P.; Hoffmann, F. M.; Chen, J. G.; Stacchiola, D. J., Stabilization of catalytically active Cu+ surface sites on titanium-copper mixed-oxide films. *Angew. Chem. Int. Ed.* **2014,** *126* (21), 5440-5444.
39. Lee, Y.-L.; Kleis, J.; Rossmeisl, J.; Shao-Horn, Y.; Morgan, D., Prediction of solid oxide fuel cell cathode activity with first-principles descriptors. *Energy Environ. Sci.* **2011,** *4* (10), 3966-3970.
40. Tran, K.; Ulissi, Z. W., Active learning across intermetallics to guide discovery of electrocatalysts for CO2 reduction and H2 evolution. *Nat. Catal.* **2018,** *1* (9), 696-703.
41. Zhong, M.; Tran, K.; Min, Y.; Wang, C.; Wang, Z.; Dinh, C.-T.; De Luna, P.; Yu, Z.; Rasouli, A. S.; Brodersen, P.; Sun, S.; Voznyy, O.; Tan, C.-S.; Askerka, M.; Che, F.; Liu, M.; Seifitokaldani, A.; Pang, Y.; Lo, S.-C.; Ip, A.; Ulissi, Z.; Sargent, E. H., Accelerated discovery of CO2 electrocatalysts using active machine learning. *Nature* **2020,** *581* (7807), 178-183.
42. Sushkevich, V. L.; van Bokhoven, J. A., Methane-to-methanol: Activity descriptors in copper-exchanged zeolites for the rational design of materials. *ACS Catal.* **2019,** *9* (7), 6293-6304.
43. Gani, T. Z. H.; Kulik, H. J., Understanding and breaking scaling relations in single-site catalysis: Methane to methanol conversion by FeIV═O. *ACS Catal.* **2018,** *8* (2), 975-986.
44. Zhao, Z.-J.; Gong, J., Catalyst design via descriptors. *Nat. Nanotech.* **2022,** *17* (6), 563-564.
45. Peterson, A. A.; Nørskov, J. K., Activity descriptors for CO2 electroreduction to methane on transition-metal catalysts. *J. Phys. Chem. Lett.* **2012,** *3* (2), 251-258.

46. Fu, R.; Nielsen, R. J.; Goddard, W. A.; Fortman, G. C.; Gunnoe, T. B., DFT virtual screening identifies rhodium–amidinate complexes as potential homogeneous catalysts for methane-to-methanol oxidation. *ACS Catal.* **2014,** *4* (12), 4455-4465.
47. Liao, W.; Liu, P., Enhanced descriptor identification and mechanism understanding for catalytic activity using a data-driven framework: revealing the importance of interactions between elementary steps. *Catal. Sci. Tech.* **2022,** *12* (12), 3836-3845.
48. Rosenzweig, A. C.; Frederick, C. A.; Lippard, S. J.; Nordlund, P.; auml, Crystal structure of a bacterial non-haem iron hydroxylase that catalyses the biological oxidation of methane. *Nature* **1993,** *366* (6455), 537-543.
49. Ross, M. O.; MacMillan, F.; Wang, J.; Nisthal, A.; Lawton, T. J.; Olafson, B. D.; Mayo, S. L.; Rosenzweig, A. C.; Hoffman, B. M., Particulate methane monooxygenase contains only mononuclear copper centers. *Science* **2019,** *364* (6440), 566-570.
50. Balasubramanian, R.; Smith, S. M.; Rawat, S.; Yatsunyk, L. A.; Stemmler, T. L.; Rosenzweig, A. C., Oxidation of methane by a biological dicopper centre. *Nature* **2010,** *465* (7294), 115-119.
51. Scott, S. L., Bioinspired methane oxidation in a zeolite. *Science* **2021,** *373* (6552), 277.
52. Snyder, B. E. R.; Vanelderen, P.; Bols, M. L.; Hallaert, S. D.; Böttger, L. H.; Ungur, L.; Pierloot, K.; Schoonheydt, R. A.; Sels, B. F.; Solomon, E. I., The active site of low-temperature methane hydroxylation in iron-containing zeolites. *Nature* **2016,** *536*, 317.
53. Göltl, F.; Michel, C.; Andrikopoulos, P. C.; Love, A. M.; Hafner, J.; Hermans, I.; Sautet, P., Computationally exploring confinement effects in the methane-to-methanol conversion over iron-oxo centers in zeolites. *ACS Catal.* **2016,** *6* (12), 8404-8409.
54. Hammond, C.; Forde, M. M.; Ab Rahim, M. H.; Thetford, A.; He, Q.; Jenkins, R. L.; Dimitratos, N.; Lopez-Sanchez, J. A.; Dummer, N. F.; Murphy, D. M.; Carley, A. F.; Taylor, S. H.; Willock, D. J.; Stangland, E. E.; Kang, J.; Hagen, H.; Kiely, C. J.; Hutchings, G. J., Direct catalytic conversion of methane to methanol in an aqueous medium by using copper-promoted Fe-ZSM-5. *Angew. Chem. Int. Ed.* **2012,** *51* (21), 5129-5133.
55. Sushkevich, V. L.; Palagin, D.; Ranocchiari, M.; van Bokhoven, J. A., Selective anaerobic oxidation of methane enables direct synthesis of methanol. *Science* **2017,** *356* (6337), 523-527.
56. Tomkins, P.; Ranocchiari, M.; van Bokhoven, J. A., Direct conversion of methane to methanol under mild conditions over Cu-zeolites and beyond. *Acc. Chem. Res.* **2017,** *50* (2), 418-425.
57. Pappas, D. K.; Borfecchia, E.; Dyballa, M.; Pankin, I. A.; Lomachenko, K. A.; Martini, A.; Signorile, M.; Teketel, S.; Arstad, B.; Berlier, G.; Lamberti, C.; Bordiga, S.; Olsbye, U.; Lillerud, K. P.; Svelle, S.; Beato, P., Methane to methanol: Structure–activity relationships for Cu-CHA. *J. Am. Chem. Soc.* **2017,** *139* (42), 14961-14975.
58. Narsimhan, K.; Iyoki, K.; Dinh, K.; Román-Leshkov, Y., Catalytic oxidation of methane into methanol over copper-exchanged zeolites with oxygen at low temperature. *ACS Central Sci.* **2016,** *2* (6), 424-429.
59. Grundner, S.; Markovits, M. A.; Li, G.; Tromp, M.; Pidko, E. A.; Hensen, E. J.; Jentys, A.; Sanchez-Sanchez, M.; Lercher, J. A., Single-site trinuclear copper oxygen clusters in mordenite for selective conversion of methane to methanol. *Nat. Commun.* **2015,** *6*, 7546.
60. Mahyuddin, M. H.; Staykov, A.; Shiota, Y.; Yoshizawa, K., Direct conversion of methane to methanol by metal-exchanged ZSM-5 zeolite (metal = Fe, Co, Ni, Cu). *ACS Catal.* **2016,** *6* (12), 8321-8331.

61. Arvidsson, A. A.; Zhdanov, V. P.; Carlsson, P.-A.; Gronbeck, H.; Hellman, A., Metal dimer sites in ZSM-5 zeolite for methane-to-methanol conversion from first-principles kinetic modelling: is the [Cu-O-Cu]2+ motif relevant for Ni, Co, Fe, Ag, and Au? *Catal. Sci. Tech.* **2017,** *7* (7), 1470-1477.
62. Xie, J.; Jin, R.; Li, A.; Bi, Y.; Ruan, Q.; Deng, Y.; Zhang, Y.; Yao, S.; Sankar, G.; Ma, D.; Tang, J., Highly selective oxidation of methane to methanol at ambient conditions by titanium dioxide-supported iron species. *Nat. Catal.* **2018,** *1* (11), 889-896.
63. Harrath, K.; Yu, X.; Xiao, H.; Li, J., The key role of support surface hydrogenation in the CH4-to-CH3OH selective oxidation by ZrO2-supported single-atom catalyst. *ACS Catal.* **2019**.
64. Kwon, Y.; Kim, T. Y.; Kwon, G.; Yi, J.; Lee, H., Selective activation of methane on single-atom catalyst of rhodium dispersed on zirconia for direct conversion. *J. Am. Chem. Soc.* **2017,** *139* (48), 17694-17699.
65. Zuo, Z.; Liu, S.; Wang, Z.; Liu, C.; Huang, W.; Huang, J.; Liu, P., Dry reforming of methane on single-site Ni/MgO catalysts: Importance of site confinement. *ACS Catal.* **2018**, 9821-9835.
66. Song, Y.; Ozdemir, E.; Ramesh, S.; Adishev, A.; Subramanian, S.; Harale, A.; Albuali, M.; Fadhel, B. A.; Jamal, A.; Moon, D.; Choi, S. H.; Yavuz, C. T., Dry reforming of methane by stable Ni–Mo nanocatalysts on single-crystalline MgO. *Science* **2020,** *367* (6479), 777-781.
67. Liu, H.; Qin, Y.; Li, L.; Wang, H.; Zhu, X.; Ge, Q., CH3 radical-mediated direct methane to methanol conversion over CuO supported on rutile oxides. *J. Catal.* **2024,** *431*, 115388.
68. Orozco, I.; Huang, E.; Mahapatra, M.; Kang, J.; Shi, R.; Nemšák, S.; Tong, X.; Senanayake, S. D.; Liu, P.; Rodríguez, J. A., Understanding methanol synthesis on inverse ZnO/CuOx/Cu catalysts: Stability of CH3O species and dynamic nature of the surface. *J. Phys. Chem. C* **2021,** *125* (12), 6673-6683.
69. Liu, H.; Li, L.; Qin, Y.; Wang, H.; Zhu, X.; Ge, Q., Synergetic C–H bond activation and C–O formation on CuOx facilities facile conversion of methane to methanol. *Appl. Surf. Sci.* **2023,** *627*, 157283.

TOC Graphic

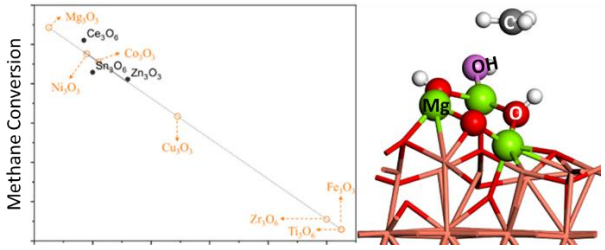
Methane Conversion
Mg_2O_3
Ce_2O_6
Co_2O_3
Sn_2O_6
Zn_2O_3
Ni_2O_3
Cu_2O_3
Fe_2O_3
Zr_2O_6
Ti_2O_6
C
OH
Mg
O